Journal of Unconventional Oil and Gas Resources 14 (2016) 99–112

Contents lists available at ScienceDirect

Journal of Unconventional Oil and Gas Resources

journal homepage: www.elsevier.com/locate/juogr

An investigation of factors affecting the interaction of CO_2 and CH_4 on shale in Appalachian Basin

Lei Hong [a,b,*], Jinesh Jain [a,b], Vyacheslav Romanov [a], Christina Lopano [a], Corinne Disenhof [a,c], Angela Goodman [a], Sheila Hedges [a], Daniel Soeder [a], Sean Sanguinito [d], Robert Dilmore [a]

[a] U.S. Department of Energy, National Energy Technology Laboratory, 626 Cochrans Mill Road, Pittsburgh, PA 15236, United States
[b] AECOM, 626 Cochrans Mill Road, Pittsburgh, PA 15236, United States
[c] AECOM, 1450 Queen Ave SW, Albany, OR 97321, United States
[d] ORISE Program, National Energy Technology Laboratory, U.S. Department of Energy, 626 Cochrans Mill Road, Pittsburgh, PA 15236, United States

ARTICLE INFO

Article history:
Received 12 November 2015
Revised 22 January 2016
Accepted 22 February 2016
Available online 25 March 2016

Keywords:
CO_2 storage and sequestration
Enhanced gas recovery
Methane
Adsorption
Shale
Gas reservoirs
Statistical analysis

ABSTRACT

Depleted unconventional gas reservoirs have been proposed reservoirs for long-term storage of anthropogenic CO_2. The injection of CO_2 in such reservoirs may benefit from, (1) the presence of existing infrastructure and right-of-way to reduce sequestration costs, (2) the presence of an existing network of fractures to increase reservoir contact efficiency, and (3) potential to enhanced gas recovery using CO_2. However, there remain significant technical challenges and uncertainties about the behavior of these reservoirs, and how they might respond to CO_2 flooding. Toward addressing those uncertainties, the present study considers results of select experiments intended to improve understanding of the fundamental characteristics of shale matrix and shale interactions with methane and carbon dioxide. Outcrop samples from the low permeability sedimentary Marcellus formations in the Appalachian Basin of the eastern United States were characterized using various analytical techniques, including FTIR, XRD, ICP-OES, TOC analyzer, surface analysis, and pycnometry. FTIR confirmed CO_2 adsorption by appearance of an absorption band near 2349 cm^{-1}, however, CH_4 absorption band at 1303 cm^{-1} was comparatively weak. Total organic carbon (TOC) exhibits significant statistical correlation with Cu, K, and Ni, while several other metals (As, Ba, Ca, Cd, Co, Cr, Fe, Mg, Mn, Na, Sr, and Ti) correlated with total inorganic carbon (TIC). Shale adsorption capacities of both CO_2 and CH_4 showed linear relationships to the organic matter content with CO_2 exhibiting consistently higher adsorption capacities than CH_4. At organic matter content greater than 2 wt%, the ratios of adsorption capacity of CO_2 over CH_4 were in a range between 1.3 and 1.9, which is similar to the ratios of critical temperatures between CO_2 and CH_4. This study evaluates the role of various physical and chemical parameters on CO_2/shale and CH_4/shale interaction, and considers implications for sequestration of CO_2 in depleted shale reservoirs.

© 2016 Elsevier Ltd. All rights reserved.

1. Introduction

Organic-rich shale formations, storing significant amounts of natural gas, directly serve as source rocks for many conventional natural gas reservoirs, and also act as seals that effectively trap gas in underlying strata for many millions of year (Hosterman and Whitlow, 1981). Natural gas is generated by both early-stage biological alteration of organic matter, and by later-stage thermal maturation as organic-rich shales are deeply buried and exposed to intense heat and pressure in an oxygen-deficient environment over geologic time (Soeder, 2012).

Conventional natural gas reservoirs contain a free gas phase within natural fractures and pore spaces in a porous and permeable rock such as a limestone or sandstone. Natural gas in conventional reservoirs was generated in an underlying source rock, most commonly an organic-rich shale, and migrated into the porous reservoir over geologic time, where it was trapped. Until recently, virtually all economic natural gas production in the world came from such conventional reservoirs, where gas was able to easily flow through the pores of the rocks and produced from a vertical extraction well (Soeder, 2012).

However, large quantities of natural gas are trapped within shale source rocks. Gas in the matrix occurs as a free phase in

* Corresponding author at: U.S. Department of Energy, National Energy Technology Laboratory, 626 Cochrans Mill Road, Pittsburgh, PA 15236, United States.
E-mail address: lei.hong@netl.doe.gov (L. Hong).

http://dx.doi.org/10.1016/j.juogr.2016.02.003
2213-3976/© 2016 Elsevier Ltd. All rights reserved.

the nanopores, and as an adsorbed phase on organic materials and clay minerals (Busch et al., 2009; Soeder, 1988). The development of directional drilling and hydraulic fracturing technologies in the 1990s for producing economical amounts of natural gas from unconventional reservoirs unlocked large natural gas resources in the United States and the world (Soeder, 2012).

Shale gas wells typically produce significant quantities of natural gas immediately after completion, followed by an initial rapid decline. The decline curve flattens out over a period of several months, and the well then continues steady production at a lower rate for years to decades (Chen et al., 2014; Yang et al., 2015). The high initial production is attributed to the release of free gas from natural fractures, which have a high permeability but a low storage volume, and are rapidly depleted. The longer-term, slower production is assumed to represent gas migration into the fractures from the shale matrix. The nanopore structure of the shale matrix itself is noted for combining reasonable porosity with very low permeability (Loucks et al., 2011). Because the pore spaces in shale are so small, gas migration through the porous matrix occurs at a molecular level, with diffusion and gas slippage as the dominant processes over classical Darcy flow (Aminian and Rodvelt, 2014; Klinkenberg, 1941).

Shale gas wells are abandoned when they no longer be produce at an economic flowrate, or when reservoir pressures have dropped to the point where formation water migrates in and separates the gas phases into isolated pockets that are no longer mobile. Such depleted shale gas reservoirs have been proposed as candidates for geologic storage of CO_2 and potential enhanced gas recovery (EGR) (Godec et al., 2014; Narinesingh and Alexander, 2014; Nuttal et al., 2005; Orr, 2009; Schepers et al., 2009; Zhang et al., 2011, 2014). The presence of a pre-existing engineered fracture network, surface infrastructure and right-of-way may help to partially offset cost associated with this storage option, and the broad spatial distribution of these wells may make them attractive targets for nearby industrial emitters. In addition, presence of unstimulated, low permeability shale above the engineered fracture network, and adsorption of CO_2 onto shale surfaces will help to ensure that injected CO_2 remains geologically stored.

Previous studies have shown that organic-rich shales have significant CO_2 adsorption capacity, and that preferential sorption of CO_2 may also enhance recovery of adsorbed methane. The adsorption capacity of CO_2 in shale has been found to be greater than that of methane (CH_4), in previous studies. For example, Kang et al. (2011), reported that CO_2 adsorption is 5–10 times greater than the adsorption of CH_4 on the Barnett Shale. Similarly, Nuttal et al. (2005) measured CH_4 and CO_2 adsorption on Devonian black shales from Kentucky and found CO_2 adsorption capacity to be 5 times that of CH_4. The results suggested that such organic-rich shale could serve to sequester carbon for long-term storage and generate enhanced CH_4 production. Godec et al. (2014, 2013) estimated the potential for EGR and CO_2 storage in the Marcellus Shale in the eastern United States, including New York, Pennsylvania, West Virginia and Eastern Ohio. In their calculation, they assumed that CO_2 displaces CH_4 with a preferential volumetric ratio of 3. The results showed that a 7% enhancement in methane production is achieved, increasing ultimate recovery efficiency to 32% of original gas in place. Using this recovery efficiency, the entire amount of recoverable methane and CO_2 storage capacity were estimated to be 12 trillion cubic meters and 5.5 billion tonnes, respectively. Schaef et al. (2014) investigated CO_2 storage and EGR by using a set of *in situ* experimental techniques. They reported that CO_2 has preferential adsorption over CH_4 on montmorillonites (a class of clay minerals commonly found in shale formations that contribute to gas sorption) at pressures under 100 bar. A maximum adsorption capacity was observed for CO_2 but not for CH_4, within the pressure range between 80 and 100 bar. The authors observed that CO_2 adsorption increases until a CO_2 monolayer formed and then desorption occurs with further increase in CO_2 pressure. It was also noted that montmorillonites undergo volumetric change during exposure to CO_2, because of the intercalation mechanism, but exposure to CH_4 does not change clays' volumes. This experimental and simulation study indicated that specific-site-based, optimized injection strategies are required to maximize CH_4 production, improve fluid transmissivity, and effectively store CO_2.

Published sorption data on shale from the Appalachian Basin, for either methane or carbon dioxide, are scarce. A comprehensive understanding of gas sorption and other petrophysical properties of shale is crucial to better understand the potential for economical EGR and carbon dioxide storage in depleted shale gas reservoirs. The objectives of this effort were to develop insights into important attributes of organic-bearing shale samples collected from seven locations around the perimeter of the Marcellus formation. These samples were characterized experimentally using a variety of analytical techniques. Adsorption isotherms of CO_2 and CH_4 on the shale samples were measured at the simulated reservoir temperature, 76.1 °C. Using these data, a preliminary investigation of relationships between the geochemical properties and adsorption properties of CO_2 and CH_4 was performed.

2. Sample collection and description

Samples were collected at seven geographic locations in West Virginia, Pennsylvania, and New York from outcrops of the Middle Devonian Marcellus Shale. The location information and description of the samples are listed in Table 1; a map of those sample locations can be found in Fig. S1 (Supporting Information). Samples represent all six of the identified lithofacies of the Marcellus Shale.

The Marcellus Shale is typically subdivided into three primary members that extend throughout the Appalachian Basin (Walker-Milani, 2011). These are the basal Union Springs Member, an organic-rich, black, silica-rich, clay poor, silty unit that contains a number of volcaniclastic deposits known as the Tioga ash beds (Roen and Hosterman, 1982). Above this is a relatively thin, organic-rich limestone identified as the Cherry Valley Member in New York, and thought to extend at least as far south as northern West Virginia based on drill core data (de Witt et al., 1993). Another limestone called the Purcell (Cate, 1963) occurs within the Marcellus in southern Pennsylvania and West Virginia. This may correspond with the Cherry Valley Limestone identified in northern portions of the basin, though there remains some debate on this (Cate, 1963; Repetski et al., 2012). The upper unit of the Marcellus formation is the Oatka Creek Member, a clay-rich, fissile shale that is highly organic at the base, and leaner toward the top. It also contains abundant ball or lens-shaped concretions, ranging from a few centimeters to more than a meter in diameter, and are usually composed of siderite, an iron carbonate mineral. The Oatka Creek Member grades upward into the overlying Mahantango Shale, gradually getting less organic and grayer in color. This upper contact of the Marcellus and Mahantango shales is gradational, and difficult to recognize in outcrops or cores.

Within this established stratigraphy, six different, smaller-scale lithofacies have been identified in the Marcellus Shale in West Virginia that are characterized by various depositional processes such as water energy, depth, terrigenous sediment supply, oxygen levels, and other factors (Walker-Milani, 2011). The lithofacies are numbered and described as follows: Facies 1 and 2 are calcareous gray shale and shaly limestone, which are interpreted as having accumulated in shallow, oxygen-rich water. Facies 3 is a calcareous black shale. Facies 4 is a noncalcareous, organic carbon-rich black shale, which is interpreted as having accumulated in anoxic bottom water. Facies 5 is a silty, dark-gray shale

Table 1
Sample information and description.

Sample suffix	Location	Stratigraphy	Description
F5	Petersburg, WV	Marcellus Shale, WV outcrop lithofacies #5	Silty, gray shale, fissile and friable, pencil fractures, bulk outcrop sample from scarp in highway department yard
F3	Petersburg, WV	Marcellus Shale, WV outcrop lithofacies #3	Calcareous, organic-rich black shale, bulk outcrop sample from roadcut
F4	Whip Gap, WV	Marcellus Shale; WV outcrop lithofacies #4	Non-calcareous, sooty black shale, stratigraphically equivalent to the basal Union Springs Member, near-vertical beds, deformed, bulk outcrop sample from valley wall of Whip Creek
F1	Burlington, WV	Marcellus Shale, WV outcrop lithofacies #1	Calcareous, organic-lean shale, bulk outcrop sample in roadcut
F2	Burlington, WV	Marcellus Shale, WV outcrop lithofacies #2	Shaly limestone, roadcut bulk outcrop sample (slab) from which oriented plugs were cut
Bedford	Bedford Co., PA	Union Springs Member of the Marcellus Shale with Tioga ash beds	Silica rich, noncalcareous black shale, bulk outcrop sample (slab) from commercial shop excavation which oriented plugs were cut, basal Marcellus Shale
OCSC	Canoga, NY	Oatka Creek Member of Marcellus Shale	Bulk outcrop sample from fresh exposure of Marcellus Shale in a limestone quarry near Canoga, Seneca Co., NY
USSC	Canoga, NY	Union Springs Member of Marcellus Shale	Bulk outcrop sample from fresh exposure of Marcellus Shale in a limestone quarry near Canoga, Seneca Co., NY
Type	Marcellus, NY	Type section Marcellus Shale (Middle Devonian)	Bulk outcrop sample of clay-rich, fissile black shale containing numerous siderite concretions in valley wall exposure of Ninemile Creek
Oatka	LeRoy, NY	Type locality of the Oatka Creek Member, Marcellus Shale	Exposure in the streambed of Oatka Creek in the town of LeRoy, NY. Clay rich, black shale with concretions downstream. Bulk outcrop sample – slab from stream bottom; hydrocarbon odor on fresh surface

containing less organic matter due to a higher rate of sediment supply compared to facies 3 or 4. Facies 6 is the volcaniclastic Tioga ash, which occurs near the base of the Marcellus Shale.

Samples "F1 and F2" were both collected from an outcrop east of Burlington, Mineral County, WV. F1 is an organic-lean, calcareous shale stratigraphically equivalent to the upper part of the Oatka Creek Member, while F2 is a shaly limestone stratigraphically equivalent to the Purcell or Cherry Valley Limestone member. Both sample F1 and F2 contain significant carbonate, some of which may be concretions or rip up clasts.

Sample "F3" was collected from a road cut along WV Route 42 north of Petersburg, Grant County, WV. F3 is characterized as a calcareous, fissile, organic-rich black shale unit. F3 is placed stratigraphically below F4, but is not considered to be a black version of the calcareous Need more Shale that lies below the Marcellus. F3 was formed during the early stages of Marcellus deposition as a calcareous to non-calcareous transition zone.

Sample "F4" lies above the Needmore Shale at Whip Gap, Grant County, WV and is a very black and sooty shale, containing more clay than most other exposures of the basal Marcellus Shale. Deformation is intense at this location, which is just to the east of and close to the Allegheny Front. The rocks are dipping nearly vertically.

Sample "F5" was collected from an exposure along WV Route 55 a short distance west of Petersburg, Grant County, WV. The F5 facies lies stratigraphically above F4, and consists of silty, clay-poor, dark gray shale. It contains less organic material than most of the basal Marcellus Shale. The sample is very friable, easily breaking into long, thin pieces known as "pencil" fractures.

Sample "Bedford" is from an exposure of basal Marcellus Shale located on Quaker Valley Road near Fishertown, Bedford Co., PA. The Bedford outcrop consists of the highly-organic, silica-rich Union Springs Member of the Marcellus Shale containing several notable Tioga ash beds (F6) within it.

Samples "OCSC" and "USSC" were obtained from exposures in the Seneca Stone Corporation quarry near Canoga, Seneca County, NY. Fresh and mostly unweathered samples were collected from quarry walls above the Onondaga Limestone. Sample OCSC represents the Oatka Creek Member from Seneca County, and sample USSC represents the Union Springs Member from Seneca County.

Sample "Type" was collected at the Marcellus Shale type locality at Slate Hill along State Highway 174/175, about a mile south of the town of Marcellus, Onondaga County, NY. The lithology of the outcrop consists of clay-rich and highly fissile black shale, with abundant siderite concretions near the base. The sample consisted of mostly intact shale, concretions and some chips.

Sample "Oatka" was collected from the streambed exposure of the Oatka Creek Member of the Marcellus Shale in LeRoy, Genesee Co., NY. The shale is exposed in the creek bottom downstream of the Main Street Bridge. Samples were collected from streambed slabs. The rock consists of clay-rich, black shale characterized by well-developed jointing and numerous, bowling-ball size concretions, similar to those present in the type section outcrop near Marcellus, NY. Freshly broken surfaces at this location have a distinct odor of hydrocarbons.

Samples were collected from either weathered outcrop exposures or fresh excavation surfaces; no attempt was made to remove residual fluids from those samples prior to testing. As such, the saturation state and composition of saturating fluids was uncontrolled, but assumed to have partial saturation with meteoric water, small to negligible amounts of hydrocarbon, and the balance as air. Sample "Oatka" from LeRoy, NY was, for example, observed to have an oily scent on freshly exposed surfaces. Natural gas producing parts of the Marcellus Shale from deeper in the basin would, in contrast, be unweathered, and contain significant saturation of hydrocarbon with likely small saturation of saline connate water (formation brine) in the pores. Outcrop samples taken from the basin margin can never be fully representative of gas productive shale from the basin center. However, access to well-preserved Marcellus Shale drill cores is extremely limited. High-quality outcrop samples were used in this study in lieu of drill cores with the assumption that the careful documentation and geologic characterization of those samples can still provide data that are relevant to the bulk of formation.

3. Experimental

3.1. Fourier Transform Infrared Spectroscopy (FTIR)

Shale samples were analyzed using two attenuated total reflectance (ATR) cells from Spectra Tech on FTIR (Figs. S2 and S3, Supporting Information). The ATR sampling technique includes two stainless steel cells connected in tandem via 0.16 cm stainless steel tubing. This design allows that the two cells experience equal

pressure. The pressure limit for the cells is 13.8 MPa. Each cell is installed with a cylindrical zinc selenide (ZnSe) ATR crystal with a length of 2.8 cm and the diameter of 0.6 cm. The incidence angle of light is set at 45° and there are eleven reflections before the light passes through the cells. The temperature of the cells is controlled by a heating jacket.

In a typical FTIR experiment, one ZnSe ATR crystal is coated with the shale sample leaving the other to act as a blank. During the experiment gaseous CH_4 and/or CO_2 was introduced to both cells at 50 °C with an increasing pressure from 0 to ~10 MPa and spectra were recorded from both cells. By subtracting the spectrum obtained from the gas-only cell from the spectrum obtained from the cell containing the shale sample, the absorption bands of CH_4 or CO_2 which is adsorbed on the shale sample can be calculated.

3.2. X-ray diffraction

Shale samples were characterized for principal mineral composition through XRD analyses. For bulk analysis, a portion of each shale sample was ground to powder using a Spex Sample Prep Shatterbox swing mill for 15 s in a tungsten carbide container. The powders were analyzed in aluminum sample holders on a Rigaku Ultima-III X-ray diffractometer using Cu K-alpha radiation from 3 to 90° two-theta (2θ). Mineral identification was performed using JADE 9 software and the International Centre for Diffraction Data PDF4+ database. Weight percent estimates were obtained for each sample using JADE 9.3's Whole Pattern Fitting software. Due to the nature of the analyses, weight percentages reported are semi-quantitative.

Four samples (F1, F5, F3, and Type) were chosen as being representative of compositional variability for identification of clay minerals. Following preparation techniques for clay analysis outlined by Poppe et al. (2001), the initial splits of crushed rock were ground to powder using a mortar and pestle to avoid potential destruction of clays, and the powders were then separated via gravity settling to obtain a sample with particles less than 5 microns. The resulting clay slurries were dried on glass slides in a low-temperature oven (~50 °C) and allowed to cool before XRD scans were conducted. Clay slides were analyzed from 3 to 30° 2θ on the same instrument as the bulk samples. After the first analysis, each slide was saturated with ethylene glycol by exposure to vapor for at least 16 h. A second XRD analysis with the same instrument settings was performed immediately after removal from the ethylene glycol.

3.3. Elemental analysis

Powdered samples were digested using lithium metaborate fusion and were analyzed by inductively coupled plasma atomic emission spectrometry (ICP-AES).

Approximately 0.1 g of powdered sample was mixed with 0.9 g of lithium metaborate in a platinum crucible and fused in a muffle furnace at 1000 °C for 30 min. The crucible, containing molten mass, was cooled and immersed in a beaker containing 5% HNO_3. The beaker was placed on a hot plate and stirred at a moderate rate until contents of the crucible were dissolved. The resulting solution was transferred to a volumetric flask and made up to 100 ml by the addition of 5% HNO_3.

A Perkin Elmer model Optima 3000 XL ICP-AES was used for all data acquisition. Samples were introduced using a peristaltic pump at 1.0 ml per minute in conjunction with an auto sampler. Analysis was performed using an external calibration procedure, and internal standards were included to correct for matrix effects and instrumental drift correction (McGinnis et al., 1997). Reference materials BIR-1 and SGR-1 were included for quality control purposes and procedural blanks were analyzed to check for any contribution from the reagents.

3.4. Carbon analysis

The analysis of carbon was performed using a CM5015 Carbon Dioxide Coulometer (UIC, Inc.) equipped with both acidification module and furnace assembly. The working range of the UIC CO_2 coulometer is from less than one microgram carbon (μg C) up to 10,000 mg for a single sample with 1000–3000 μg C being the optimal carbon concentration. However, actual quantization limits for the analysis also depend on reproducibility of sample blanks, sample size, effective removal of potential interfering species, and process parameters such as adequate CO_2 release and titration times for each sample type. Sample sizes for the individual Marcellus Shale samples tested were adjusted so that the determinations were performed within the optimal range whenever possible. NETL's largest available sample boat could only handle ~1 g of the powdered shale. Blank reproducibility with current cleaning procedures is estimated to be ±10–15 μg C which implies a quantization limit of ~15 ppm for these tests. Total inorganic carbon (TIC), i.e. carbon from the carbonate mineral content, was determined by acidification of the sample (reaction with excess 2 N $HClO_4$) followed by electrochemical titration of the released CO_2 in the coulometer cell. Three replicate TIC determinations were performed for each shale sample.

Total carbon (TC) was determined by burning the sample at 900 °C in pure oxygen in the furnace apparatus followed by electrochemical titration of the released CO_2. Four replicate TC determinations were performed for each shale sample. Total organic carbon (TOC) was determined by subtraction of the average TIC content for each shale sample from its corresponding average TC values.

3.5. Surface area measurements

Surface areas for the shale samples were measured by nitrogen adsorption using a Tristar® II 3020 analyzer from Micromeritics Instrument Corporation. Subsamples of each shale sample were ground to powders using a Spex SamplePrep Shatterbox swing mill for 15 s in a tungsten carbide container. Samples (100–150 mg) were degassed under vacuum at 99.85 °C overnight to remove moisture. Nitrogen adsorption isotherms were collected at −195.85 °C. Multipoint BET (Brunauer–Emmett–Teller) surface areas were calculated from the relative pressure (P/P_0) between 0 and 0.3. The micropore surface areas were calculated from the Dubinin–Radushkvich equation (Eq. (1)) using a pressure range between 0.02 and 0.1 MPa.

$$\log V = \log V_0 - \left(\frac{BT^2}{\beta}\right)\log^2\left(\frac{P_0}{P}\right) \quad (1)$$

where V is the volume adsorbed at equilibrium pressure P (cm^3/g STP), V_0 is the micropore capacity (cm^3/g STP), P_0 is the saturation vapor pressure of gas at temperature T (mmHg), β is the affinity coefficient of the adsorbate relative to nitrogen (for this application β is set to 1), B is a constant, and T is the analysis bath temperature (K).

3.6. Density and porosity measurements

The grain and bulk densities were measured by an AccuPyc II 1340 Series Pycnometer and porosity was determined by mercury intrusion using an AutoPore IV 9500, both these analyzers are also from Micromeritics Instrument Corp.

3.7. Adsorption capacity of CO_2 and CH_4

The adsorption capacity measurements for pure CO_2 and CH_4 were performed by Weatherford Laboratories (16161 Table Mountain Parkway Golden, Colorado 80403). A standard manometric adsorption isotherm setup was utilized except for downstream plumbing modifications for gas chromatography measurements. This setup includes large reference and sample cell design which provides better measurement accuracy by loading larger amounts of sample and limiting the effect of dead volume, which is beneficial for low storage capacity samples such as shale. The desired temperatures were achieved by immersion of the cells in an oil bath with an accuracy of less than 0.11 °C. The temperature within the sample cell was monitored directly with a thermocouple with an accuracy of ±0.028 °C. Isotherm measurements can be performed at temperatures from 12 °C to 148 °C. The pressure transducers are directly immersed into the oil bath reducing temperature effects upon the transducers themselves. The transducers were temperature compensated with accuracy to 0.05% of full scale (34 MPa). The measurement pressure can reach up to 68.9 MPa. Pressure and temperature data were monitored and recorded by a computer data acquisition system. The isotherms were measured at 76.1 °C. The sorption data were fit to a simple Langmuir isotherm equation, as described by Zhang et al. (2012), and in other literature. Results of that fitting exercise are described in Section 4.

3.8. Statistical data analysis

In order to determine whether statistical correlation exists between any two properties characterized in this study, Pearson's product-moment correlation was applied to the experimental data using Minitab 14.1. The correlation coefficient (r) and the significance (p-value) were calculated. In general, correlation is considered to be low or weak if r (in absolute value) is less than 0.35, modest or moderate for r values from 0.36 to 0.67, and strong or high for r values at or above 0.68. (Taylor, 1990) In this study, we consider that at a p-value less than 0.05, the reported result attains statistical significance.

4. Results

4.1. Fourier Transform Infrared Spectroscopy (FTIR)

The FTIR analysis was conducted at 50 °C and different pressure settings by exposing the samples to CH_4 and CO_2 gases. The data for the sample Type after exposure with CH_4 at 9.7 MPa are shown in Fig. 1. In general, gaseous CH_4 has two infrared-active vibrational modes namely a stretching mode at 3019 cm^{-1} and a deformation mode at 1306 cm^{-1} (Li et al., 1994; "Molecular Database, The Virtual Planetary Laboratory," 2015). In our study the deformation vibrational spectra for CH_4 was observed with a slight red shift at 1303 cm^{-1}. The data presented in Fig. 1 indicate that measurement of the shale sample alone did not show any CH_4 absorption (blue spectrum). However, when the sample was exposed to gaseous CH_4 an absorption band (green spectrum) similar to CH_4 gas alone (red line) was observed at 1303 cm^{-1}. Any absorption of CH_4 (purple spectrum) on the shale sample was calculated by subtracting CH_4 spectrum (green spectrum) from the spectrum of shale plus CH_4 (red spectrum). The purple spectrum in Fig. 1 indicates that there is no identifiable adsorbed CH_4 observed in the shale sample Type due to the absence of any absorption band at or near the 1303 cm^{-1}. CH_4 absorption on other shale samples, therefore, was not studied.

Sample "Type" was also studied in terms of CO_2 adsorption at 4.2 MPa (Fig. 2). CO_2 has strong vibrational modes, located at 2349 cm^{-1} (ν_3 asymmetric stretching vibrations) and 667 cm^{-1} (ν_2 bending mode) (Krukowski et al., 2015; "Molecular Database, The Virtual Planetary Laboratory," 2015; Romanov, 2013). As indicated in Fig. 2 the split vibrational absorption band is observed for both gaseous CO_2 (red spectrum) and CO_2 plus shale sample (green spectrum) at 2349 cm^{-1}. The splitting of the band can be ascribed to the CO_2 rotational–vibrational transition, where 2349 cm^{-1} corresponds to the fundamental Q band of pure CO_2 (Martin and Barker, 1932; Romanov, 2013). Subtracting red spectrum (CO_2 alone) from the green spectrum (shale plus CO_2) produces a readily identifiable CO_2 absorption band that shale sample (purple spectrum). This observation is consistent with previous study by Romanov (Romanov, 2013).

Close-up view of FTIR spectra between 2300 and 2400 cm^{-1} was examined for CO_2 interactions with shale samples F5, F4, F2, OCSC, Type and Oatka at different pressure conditions (Fig. 3). The two CO_2 absorption bands at 2343 and 2331 cm^{-1} suggests that CO_2 has two modes of interaction in shale, which will be further discussed in Section 5.

4.2. X-ray diffraction

Table 2 shows the results for the bulk XRD analyses as estimated mass percentages of different crystalline phases (e.g. mineral content) present in the samples. Within the samples analyzed, quartz ranges from approximately 17% of the total mineral content in F2 to 88% in F4. Eight of the samples have significant amounts of identified clay minerals, which are primarily illite with some chlorite. Two samples, identified as non-calcareous black shale (Bedford) and shaly limestone (F2), contain less than 10% clays. Calcite in the sample set ranges from 3% in F5, the silty shale, to 74% in F2, the shaly limestone.

Table 2 also shows the results of clay analyses. Ethylene glycol tests confirmed that there is no smectite-group clays ($Ca(Al, Mg)_2$, $SiO_{10}(OH)_2 \cdot H_2O$) identified in the samples. Illite and chlorite are the dominant clays in the sample set with illite ranging from approximately 6% in F2 to 36% in the Oatka sample, and chlorite ranging from roughly 3% in Oatka to 12% in F5. Glycolation caused a shift in several peaks in sample F1 that may suggest a mixed-layer clay, although further analysis is needed to confirm this.

4.3. Elemental analysis

Table 3 lists the concentration of detectable elements in the samples obtained by ICP-AES. Notably, the sample F2 has extremely high concentration of barium among all the samples analyzed. One possible explanation is that the location of this sample collected was contaminated by drilling mud consisting of barite as a weighting agent (Neff et al., 2000). Relative abundance of these elements is also plotted in Fig. S4 (Supporting Information).

4.4. Carbon analysis

Table 4 lists the data for total carbon (TC), total inorganic carbon (TIC), and total organic carbon (TOC). Samples F1 and F2 were both collected from the same location and most of their carbon is in the inorganic format. Of those two samples F2 has the highest concentration of TIC. F3 is located stratigraphically below F4. Both F3 and F4 are described as black shale, and show relative higher organic carbon content than F1 and F2. All the carbon identified in sample F4 was determined to be organic. F5 is located stratigraphically above F4, and is described having less organic content than most of the basal Marcellus Shale, and F5 contains less

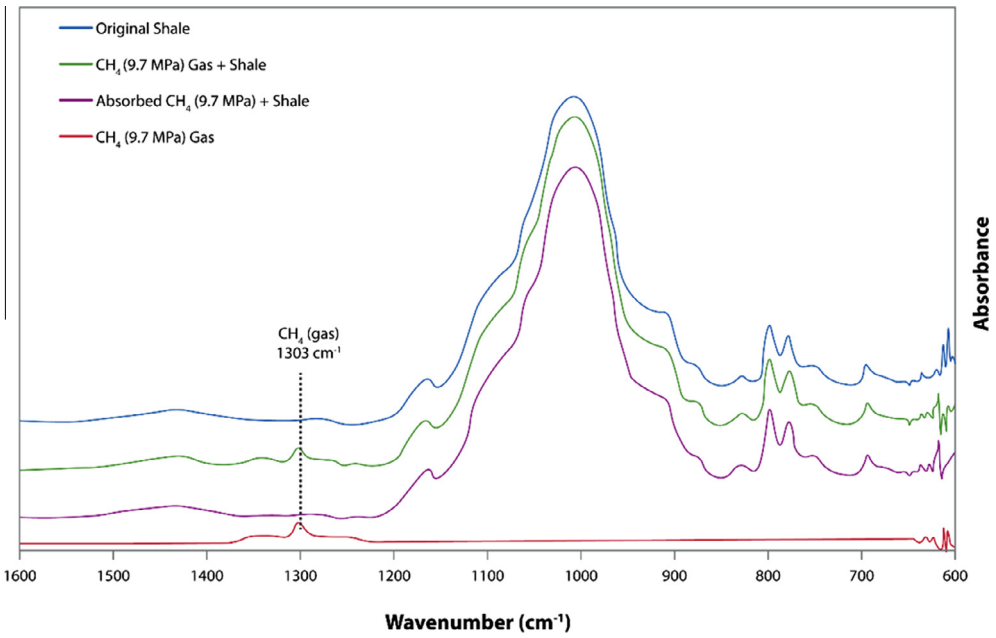

Fig. 1. FTIR spectra of sample Type after adsorbed CH_4 at 9.7 MPa.

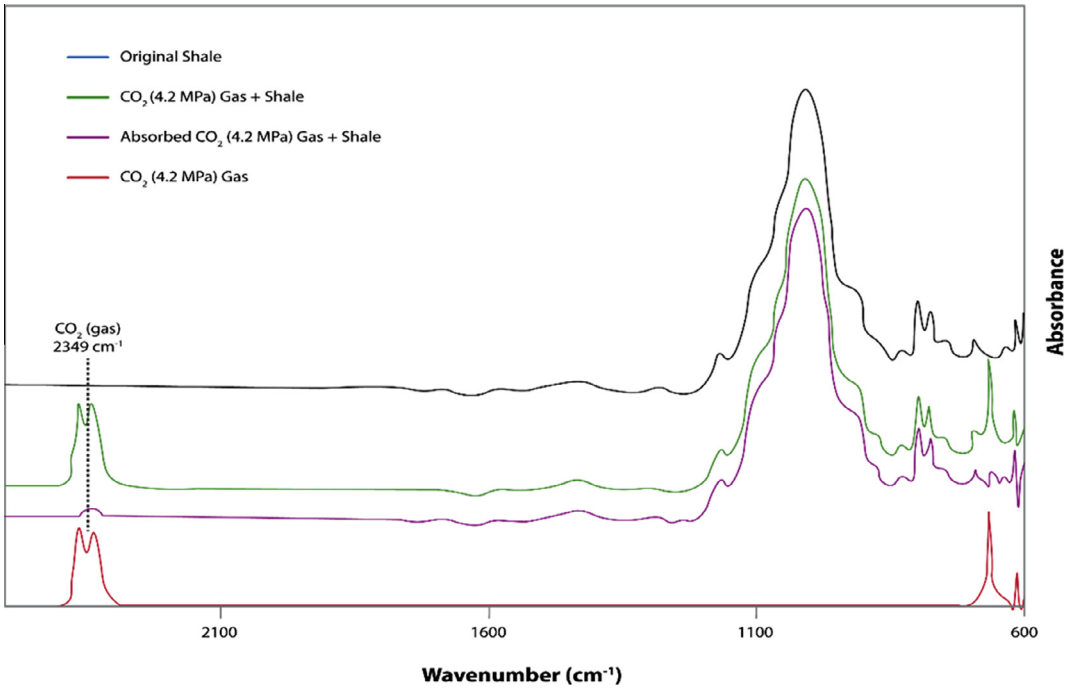

Fig. 2. FTIR spectra of shale Type after adsorbed CO_2 at 4.2 MPa.

organic carbon content than samples F3 and F4. Matching the features described in the previous section, sample Bedford contains 5.25% organic carbon, which includes within it highly-organic Union Springs Member. Sample OCSC has the highest measured concentration of TOC of all the samples (8.9 wt%), which represents the Oatka Creek Member, a highly organic shale. Sample USSC represents the Union Spring Member – another organic-rich shale. Samples "Type" and "Oatka" are also considered to be black shales, which are characterized with relative high TOC content. Sample Oatka has the second highest TOC content in all the samples.

4.5. Surface area, density and porosity

Economical and efficient shale gas production enhanced by CO_2 injection is expected to be highly dependent on understanding key rock properties such as porosity and surface area of shales.

Grain density describes the density of solid or mineral grains of a rock. In log and core analysis, the term "grain" refers to all the solid material in the rock, because no effort is made to distinguish mineral grains from other solid material when interpreting the measurements. Grain density can be a mineralogical indicator of

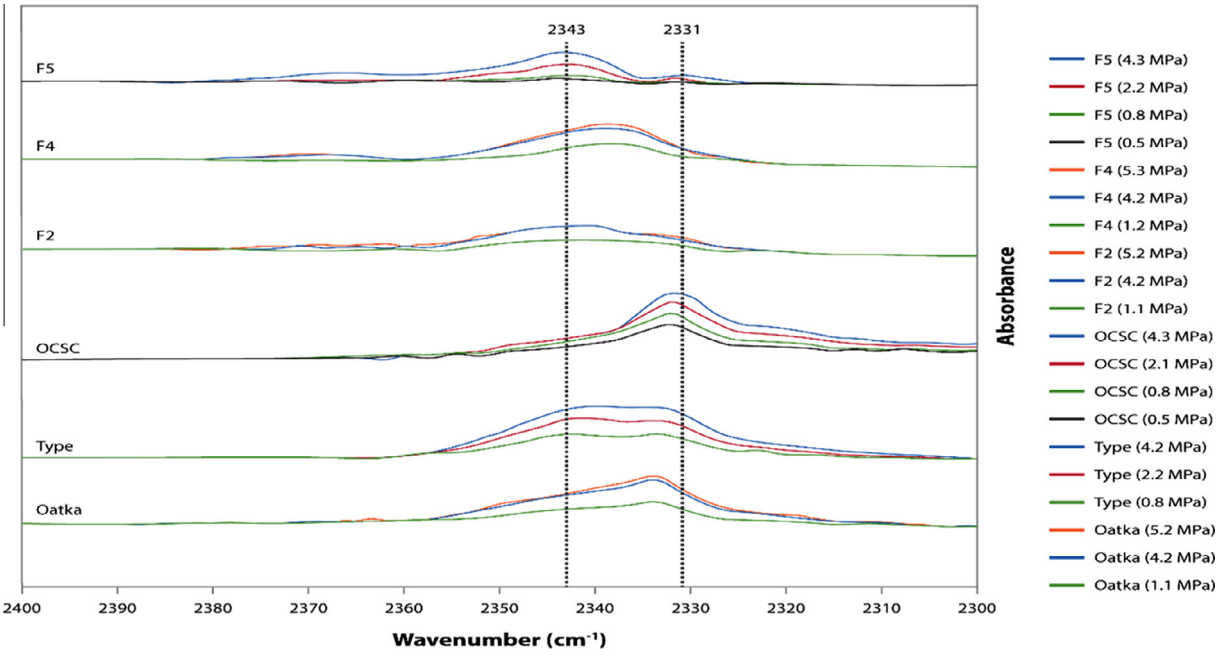

Fig. 3. FTIR spectra of the six shale samples with adsorbed CO_2 at 50 °C as a function of CO_2 pressure.

Table 2
X-ray diffraction results for the shale samples.

Sample suffix	Quartz SiO_2 (wt%)	Calcite $CaCO_3$ (wt%)	Illite/muscovite $KAl_2(AlSi_3O_{10})(OH)_8$ (wt%)	Chlorite $(Mg,Al,Fe)_6(Si,Al)_4O_{10}(OH)_8$ (wt%)	Pyrite FeS_2 (wt%)	Dolomite $CaMg(CO_3)_2$ (wt%)
F5	52	3	26	12	1	7
F3	35	37	16	6	N/A	6
F4	88	N/A	12	N/A	N/A	N/A
F1	44	14	32	10	N/A	N/A
F2	17	74	6	N/A	N/A	N/A
Bedford	74	16	7	N/A	1	3
OCSC	26	51	14	N/A	4	4
USSC	35	32	27	5	2	N/A
Type	49	4	35	7	6	N/A
Oatka	49	6	36	3	7	N/A

Note: N/A represents that the constitute is not detectable in X-ray diffraction.

the rock because the density varies with the mineral composition of the rock and the state of hydration of the minerals. Bulk densities are important in quantitative soil studies.

The surface area, density, and porosity data of the samples are listed in Table 5. Sample OCSC has the largest BET area, and sample F2 has the smallest. In general, grain density is larger than bulk density because the grain density is mostly determined by mineral components of the shale, which has higher density than non-mineral components. All samples except sample F3 have higher grain density than bulk density. F5 has a median pore diameter (5.226 μm) that is an order of magnitude larger than all other samples. Sample F4 is, so far, the most porous sample with a porosity of 25.52%.

4.6. CO_2 and CH_4 adsorption

Methane and carbon dioxide adsorption isotherms are included as attachments in the Supporting Information (Figs. S5 and S6) and parameters used to generate those isotherms are given in Table 6. The maximum adsorption capacities for CO_2 and CH_4 are calculated using Langmuir isotherm equation. It is interesting to note that the CO_2 adsorption capacities for all samples is larger than the CH_4 values, suggesting that EGR process by freeing of sorbed CH_4 with injected CO_2 could be a thermodynamically viable process. There is, however, an observed trade-off between the total adsorption capacity and the ratio of CO_2 to CH_4 capacity of gas absorption. For example, the sample OCSC exhibits highest adsorption capacity for both CO_2 and CH_4; however, the capacity ratio of CO_2 to CH_4 is one of the smallest values.

4.7. Total statistical data analysis

The correlation coefficients and *p*-value calculated from any two measured properties are presented in the Supporting Information (Table S1).

5. Discussion

5.1. FTIR and XRD

Two CO_2 absorption bands observed at 2343 and 2331 cm^{-1} (Fig. 3) suggest that CO_2 interacts with shale samples by two distinct mechanisms. The band observed at 2343 cm^{-1} arises from the binding of CO_2 with inorganic sites, such as interlayer of clays (Krukowski et al., 2015; Romanov, 2013). CO_2 is also known to adsorb onto organic matter (i.e., kerogen) via Van der Waals forces,

Table 3
Elemental composition of shale samples as determined by back-calculation from measured composition in sample digestate using ICP-AES.

Element	Detection limit (μg/g)	Sample suffix (units in μg/g)									
		F5	F3	F4	F1	F2	Bedford	OCSC	USSC	TYPE	Oatka
Al	19.0	8913	4746	2125	8469	1404	2171	2974	6389	7915	7001
As	1.20	3.61	2.78	2.12	3.89	3.15	3.45	5.40	3.03	5.07	6.39
Ba	1.60	80.2	58.7	36.4	86.0	2989	21.7	19.3	42.1	44.0	32.7
Ca	51.0	1540	13459	BDL	4057	25722	6630	17178	9971	1135	1564
Cd	0.32	0.83	0.38	BDL	0.57	0.50	BDL	0.33	0.48	0.57	0.72
Co	1.7	2.22	BDL	BDL	1.86	BDL	BDL	BDL	BDL	2.62	2.61
Cr	0.70	14.6	11.9	13.8	15.4	8.65	7.63	13.2	12.4	17.1	13.9
Cu	4.00	BDL	BDL	4.4	BDL	BDL	14.7	26.9	5.7	7.56	14.4
Fe	46.0	4649	2133	707	3703	1689	968	2235	2075	4677	4260
K	188	3207	1882	864	3359	589	892	1808	3119	3675	3243
Mg	6.00	1123	933	123	874	403	384	609	882	947	851
Mn	0.60	55.4	29.4	2.3	43.5	48.1	12.6	12.9	26.9	20.9	15.3
Mo	0.20	1.19	1.92	10.9	2.48	3.89	8.77	11.5	2.54	9.83	13.6
Na	72.0	500	385	125	414	219	235	291	234	222	369
Ni	2.30	14.0	9.91	6.30	9.96	6.31	14.5	41.0	24.6	15.1	21.5
P	18.0	34.4	28.6	BDL	57.0	24.2	42.3	40.0	29.2	44.1	33.8
Pb	0.80	BDL	1.24	4.64	BDL	BDL	2.65	2.41	BDL	2.53	3.72
S	161	646	548	BDL	BDL	1333	213	518	524	998	651
Si	60.0	24,688	16,579	35,481	22,450	5582	28,738	10,708	18,054	24,757	20,482
Sr	0.60	10.5	29.4	4.70	12.9	56.6	17.7	33.1	25.1	8.74	9.56
Ti	0.05	497	311	105	452	96	104	173	345	406	259
V	0.29	13.6	8.76	40.8	14.2	3.74	32.0	43.0	14.0	20.0	28.8

Note: BDL = below detection limits.

Table 4
Carbon analysis of the Marcellus Shale samples.

Sample suffix	Total carbon (TC)		Total inorganic carbon (TIC)		Total organic carbon (TOC)	
	Average carbon (wt%)	Standard deviation	Average carbon (wt%)	Standard deviation	Average carbon (wt%)	Standard deviation
F5	1.127	0.01	0.749	0.00	0.378	0.01
F3	5.91	0.11	4.82	0.01	1.08	0.11
F4	4.02	0.15	BDL	N/A	4.02	0.15
F1	1.51	0.02	1.29	0.00	0.22	0.02
F2	9.43	0.04	8.63	0.10	0.8	0.11
Bedford	7.58	0.14	2.33	0.00	5.25	0.14
OCSC	14.73	0.06	5.82	0.07	8.9	0.10
USSC	6	0.06	3.37	0.02	2.63	0.06
Type	3.56	0.05	0.319	0.00	3.24	0.05
Oatka	8.12	0.21	0.567	0.01	7.55	0.21

Note: BDL = below detection limits.

Table 5
Surface areas, grain and bulk density, and porosity of the shale.

Sample suffix	BET surface area (m^2/g)	Grain density (g/cm^3)	Bulk density (g/cm^3)	Median pore diameter (μm)	% porosity
F5	10.4	2.79	2.76	5.226	1.98
F3	10.3	2.73	2.79	0.136	7.92
F4	8.1	2.54	1.97	0.314	25.52
F1	16.6	2.75	2.54	0.114	14.82
F2	5.7	2.79	2.67	0.009	6.73
Bedford	23.5	2.56	2.46	0.312	2.4
OCSC	33.8	2.55	2.38	0.022	2.53
USSC	18.1	2.71	2.50	0.010	3.84
Type	20.4	2.75	2.29	0.023	3.35
Oatka	7.3	2.57	2.43	0.004	3.37

Table 6
Pure gas adsorption isotherm parameters of CO_2 and CH_4 on shale samples.

Sample suffix	Maximum adsorption capacity, CH_4 (mol/kg)	Maximum adsorption capacity, CO_2 (mol/kg)	CO_2:CH_4 ratio
F5	0.02440	0.07386	3.027
F3	0.03878	0.16273	4.196
F4	0.13653	0.19632	1.4380
F1	0.04460	0.10689	2.396
F2	0.02741	0.1009	3.681
Bedford	0.14894	0.28313	1.9010
OCSC	0.29237	0.39507	1.3512
USSC	0.1034	0.19545	1.889
Type	0.12413	0.16546	1.3330
Oatka	0.23651	0.31126	1.3161

which could explain the appearance of the CO_2 band at 2331 cm^{-1}. This hypothesis is consistent with previous studies using coal where ν_3 stretching band of CO_2 was identified at 2333 cm^{-1} (Goodman, 2009). Although the data presented here cannot establish a strong correlation between the adsorption binding sites and the inorganic/organic carbon compositions, the distribution of two CO_2 absorption bands in this work is consistent with the inorganic and organic composition of shale samples presented in Table 4. The sample OCSC, which contains the highest concentration of organic carbon, shows a dominant absorption band at 2331 cm^{-1}. The sample F2 has highest amount of inorganic carbon and displays a distinct peak at 2343 cm^{-1} (Fig. 3).

XRD results (Table 2) indicate that there is no swelling clay mineral contents (i.e., smectites) observed in any of the shale samples. The swelling clays have been well studied as potential CO_2 storage sinks (Hur et al., 2013; Loring et al., 2014; Romanov,

2013) where CO_2 is incorporated into hydrated interlayers of swelling clays, facilitating the CO_2 adsorption. This type of adsorption in interlayers is considered to be negligible in this study.

5.2. Enrichment factors of metals

The customary way to estimate the authigenic enrichment of a given element is to define an enrichment factor (EF) by normalizing the measured element content with respect to the content of a reference element which is based on the average shale composition. Aluminum (Al) is commonly used as the normalization element mainly because it is an inherent and abundant component of the clay mineral structure and its concentration generally is not affected by biological or diagenetic process during the creation of geological formations. The EF is calculated according to Eq. (2) (Abrahim and Parker, 2008; Brumsack, 2006; Pi et al., 2013):

$$EF = (C_{element}/C_{Al})_{sample}/(C_{element}/C_{Al})_{average\ shale} \quad (2)$$

where $C_{element}$ and C_{Al} are the concentrations (in ppm) of the specific element and Al in the shale, respectively. The average ratio of individual element over Al can be found in the Brumsack's paper, as listed in Table 7 (Brumsack, 2006).

Vine and Tourtel (1970) suggested that the elements in black shale can be divided into following groups: (1) elements associated detrital fraction (Al, Ti, Ga, Zr, Sc), (2) elements associated with carbonate fraction (Ca, Mg, Mn, Sr), and (3) the elements most commonly associated with the organic fraction (Ag, Mo, Zn, Ni, Cu, Cr, V). Table 7 lists the ratios of detectable elements over Al and the EFs for all the shale samples analyzed. According to the definition of EF (Eq. (2)), an element is considered relatively enriched when EF is greater than 1 and depleted when EF is less than 1. It is interesting to note that the sample F2 is enriched with many elements, including As, Ba, Ca, Cd, Fe, Mg, Mn, Na, Sr, and Ti, compared to other samples. However, none of these elements is associated with organic matter, which indicates the sample F2 may contain small amount of organic matter which is supported by the total organic carbon data (Table 4). The data presented in Table 7 also show that the highest EF values for the organic-associated elements are found in both shale samples F4 and OCSC. The sample F4 is enriched in Cr, Mo, and V, comparably, the sample OCSC is enriched with Cu and Ni.

It has been shown that there is a high correlation between TOC content and the ratio of Mo/Al in those oxygen-deficient sediments (Wilde et al., 2004). A correlation of TOC as a function of Mo/Al for the euxinic black shales within the Devonian Oatka Creek Formation, New York, northern Appalachian Basin was given as TOC (%) = 2024(Mo/Al) + 3.9 (r^2 = 0.90). The TOC is plotted with Mo/Al for the samples studied in this project, as shown in Fig. 5. The correlation of those samples from New York was calculated as TOC (%) = 1920.1(Mo/Al) + 2.004 (r^2 = 0.831) (Fig. 4a), which is comparable to the correlation obtained from the literature report (Wilde et al., 2004). The correlation for the shale samples from West Virginia is calculated as TOC (%) = 837.55(Mo/Al) + 0.1753 (r^2 = 0.7223) (Fig. 4b). The correlation indicates that those shales from West Virginia experienced a different geologic history from those from New York.

5.3. Metal composition and carbon content

The detrital metals (Al, Ti, Ga, Zr, Sc) defined by Vine and Tourtel (1970) generally form a major structure of shale. These metals were mainly introduced via fluvial and eolian sources. They exist in high concentrations and more importantly their concentrations essentially are not affected by the changes in natural environments with time. Two major detrital metals Al and Ti were detected in all shale samples. However, the sample F2 has the highest EF of Ti, whereas Oatka has the lowest EF of Ti (Table 7).

As shown in Table S1 (Supporting Information), TIC appears to have a strong correlation with As, Ba, Ca, Cd, Co, Cr, Fe, Mg, Mn, Na, Sr, and Ti with respect to their small p-values ($p < 0.05$). All of these metals appear to form stable carbonate salts. The total EFs of all the TIC related metals can be calculated by adding their EF values together and the results are shown in Fig. 5. Sample F2 exhibits the highest EF correlation to TIC, which indicates that F2 is the most "inorganic"-carbon-enriched shale. This is further supported by the data presented in Table 4, which indicate that F2 has the highest TIC contents as compared to all other samples.

Table 7
Average ratio of element/Al and enrichment factors (EFs) calculated using Eq. (2) for the detectable elements in groups.

Element sample suffix	Average shale (element/Al)	Enrichment factor (EF)									
		F5	F3	F4	F1	F2	Bedford	OCSC	USSC	TYPE	Oatka
Detrital elements											
Ti	0.053	1.05	1.24	0.93	1.01	1.29	0.90	1.10	1.02	0.97	0.70
Carbonate elements											
Ca	0.18	0.96	15.75	N/A	2.66	101.78	16.97	32.09	8.67	0.80	1.24
Mg	0.18	0.70	1.09	0.32	0.57	1.59	0.98	1.14	0.77	0.66	0.68
Mn	96×10^{-4}	0.65	0.65	0.11	0.54	3.57	0.60	0.45	0.44	0.28	0.23
Sr	34×10^{-4}	0.35	1.82	0.65	0.45	11.86	2.40	3.27	1.16	0.32	0.40
Organic associations											
Mo	0.15×10^{-4}	8.90	26.97	341.96	19.52	184.71	269.31	257.79	26.50	82.80	129.51
Ni	7.7×10^{-4}	2.04	2.71	3.85	1.53	5.84	8.67	17.90	5.00	2.48	3.99
Cu	5.1×10^{-4}	N/A	N/A	4.06	N/A	N/A	13.28	17.74	1.75	1.87	4.03
Cr	10.2×10^{-4}	1.61	2.46	6.37	1.78	6.04	3.45	4.35	1.90	2.12	1.95
V	15×10^{-4}	1.02	1.23	12.80	1.12	1.78	9.83	9.64	1.46	1.68	2.74
Others											
As	1.1×10^{-4}	3.68	5.33	9.07	4.18	20.40	14.45	16.51	4.31	5.82	8.30
Ba	66×10^{-4}	1.36	1.87	2.60	1.54	322.56	1.51	0.98	1.00	0.84	0.71
Cd	0.015×10^{-4}	62.08	53.38	N/A	44.87	237.42	N/A	73.97	50.09	48.01	68.56
Co	2.1×10^{-4}	1.19	N/A	N/A	1.05	N/A	N/A	N/A	N/A	1.58	1.78
Fe	0.55	0.95	0.82	0.60	0.79	2.19	0.81	1.37	0.59	1.07	1.11
K	0.34	1.06	1.17	1.20	1.17	1.23	1.21	1.79	1.44	1.37	1.36
Na	0.13	0.43	0.62	0.45	0.38	1.20	0.83	0.75	0.28	0.22	0.41
P	0.008	0.48	0.75	N/A	0.84	2.15	2.44	1.68	0.57	0.70	0.60
Pb	2.5×10^{-4}	N/A	1.05	8.73	N/A	N/A	4.88	3.24	N/A	1.28	2.13
Si	3.11	0.89	1.12	5.37	0.85	1.28	4.26	1.16	0.91	1.01	0.94

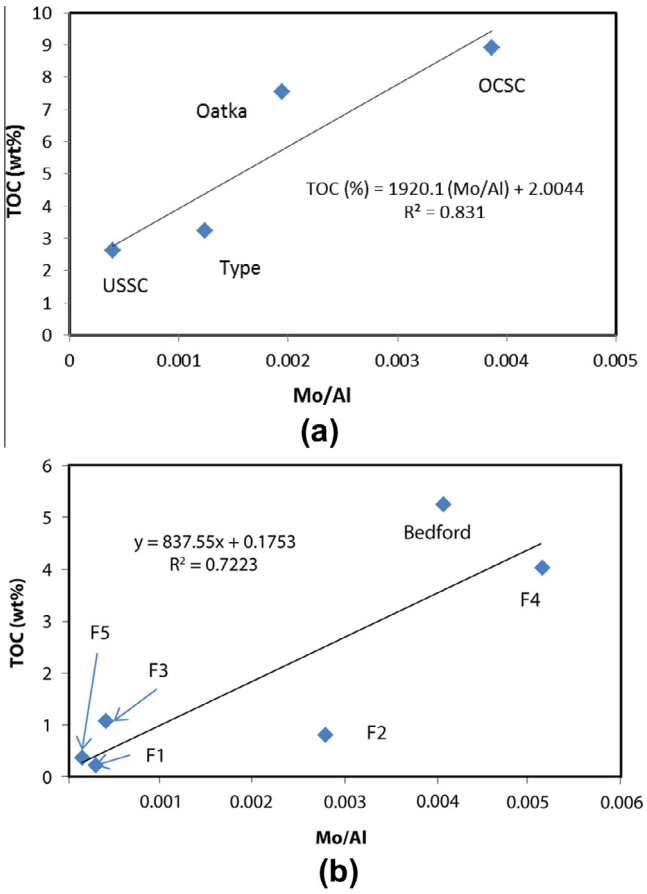

Fig. 4. TOC is plotted as a function of Mo/Al for the shale samples from (a) Oatka Creek, NY, northern Appalachian Basin; (b) West Virginia and Pennsylvania, southern Appalachian Basin.

Organic carbon in sedimentary rocks occurs in the preserved remnants of plants and animals, often enriched in specific metals (i.e., Mo, V, Cu, Zn, V) bearing a relation to their abundance in the plants, animals and even seawater. According to Table S1 (Supporting Information), TOC is strongly correlated with Cu, K, and Ni, both Cu and Ni are also located in Vine and Tourtelot's organic carbon category (Vine and Tourtel, 1970). The total ER values of organic carbon metals were calculated by adding the EFs of Cu, K and Ni and the data are also plotted in Fig. 5. It is clear from the data that the sample F4 has the largest EF of organic associated metals followed by OCSC and Bedford. Interestingly, F4 has all its carbon in organic form and no TIC was detected in this sample (Table 4). Although Samples OCSC, Bedford, and Oatka have lower EFs of the TOC related metals than F4 but the actual organic carbon contents are higher than F4 (Table 4). This type of correlation analysis establishes a general relationship between the metal enrichments and carbon content in shale.

5.4. Elemental composition and physical properties

The physical properties characterized in this study include BET area, grain density, bulk density, median pore diameter, and porosity. It is interesting to note that BET is strongly correlated with Cu, K, and Ni, which is similar to the TOC correlation with metals (Table S1 in the Supporting Information). However, the *p*-value between BET area and TOC does not support such correlation. It may be possible that the BET area includes the contributions from both TOC and organic carbon related metals. Also median pore diameter and porosity do not exhibit a correlation with any other characterized properties, including metal and sorption properties. This emphasizes that the pore characteristics in organic-rich shales is very complex, and impacted by numerous physical and geochemical processes occurring over millions of years; further studies are needed to understand the nature of shale pore structure, and the effect of pore morphology on gas adsorption and transport properties.

Densities are found to have significant correlation with the metal enrichments of the shale samples (Table S1 in the Supporting Information). While Mo, Pb, and V are correlated to both grain and bulk density, Cu is related to only grain density and Si to bulk density. It is noted that there is a slight negative correlation between the density and the metal EF, as shown in Fig. 6. Si is one of the fundamental structural elements for shales. The enrichment of Si is more correlated to bulk density than the grain density which is more dependent on mineral grains in shale.

Table S1 also shows that grain density has a positive correction with bulk density. As shown in Table 5, grain densities are generally larger than bulk densities. The bulk density counts the entire volume including all voids in shale. More grains per unit volume might fill additional voids, reducing the void volume in shale. Therefore, a higher grain density leads to a higher bulk density.

5.5. Grain density and TOC

Grain density is plotted against TOC in Fig. 7. Table S1 (Supporting Information) shows that grain density and TOC have a strong

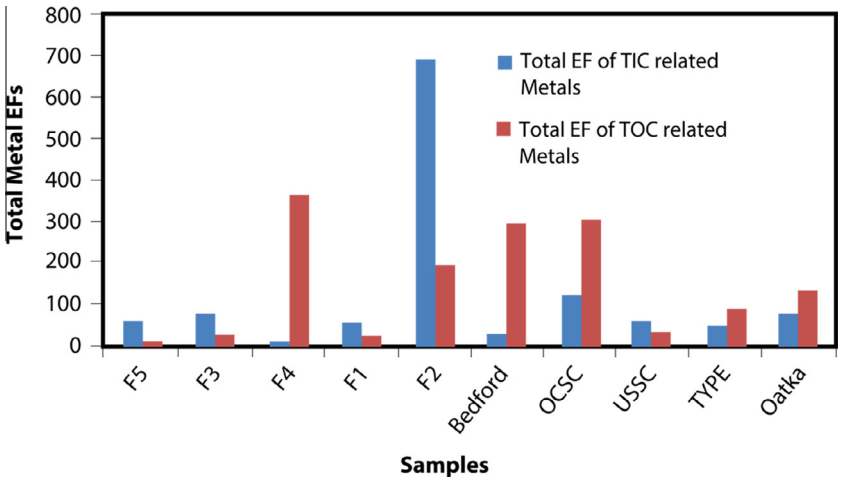

Fig. 5. Total EF of TIC and TOC related metals of all the samples.

negative correlation. Generally the densities of minerals within a rock are significantly higher than densities of the organic components. An increase in the TOC contents in a given volume might reduce the mineral content resulting in a decreased grain density.

5.6. CO_2 and CH_4 adsorption

As shown in Table S1 (Supporting Information), both CO_2 and CH_4 adsorptions are statistically correlated to the enrichment of Cu, K, and Ni, which is similar to the correlation trend between TOC and metal enrichment. Furthermore, CO_2 and CH_4 adsorptions are negatively correlated with grain density, which is similar to the correlation trend between TOC and grain density. It is not surprising to find that adsorption is strongly correlated with TOC contents in the samples (Busch et al., 2008).

The isotherms for both CO_2 and CH_4 are well fit by the Langmuir equation, which is generally accepted as a model for mono-layer adsorption at relatively low pressure conditions (Sakurovs et al., 2008, 2007). The maximum adsorption capacities of CO_2 and CH_4 are plotted against TOC percentages in Fig. 8. Both CO_2 and CH_4 sorption capacities follow a linear relationship with TOC contents with regression coefficients of 0.94 and 0.98, respectively. These results are consistent with the data reported in the literature

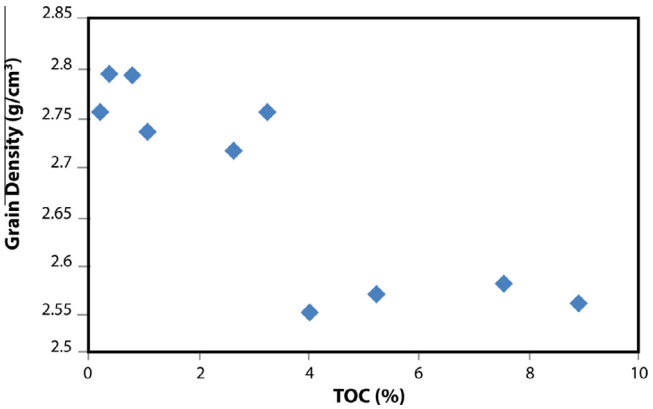

Fig. 7. TOC is plotted as a function of grain density.

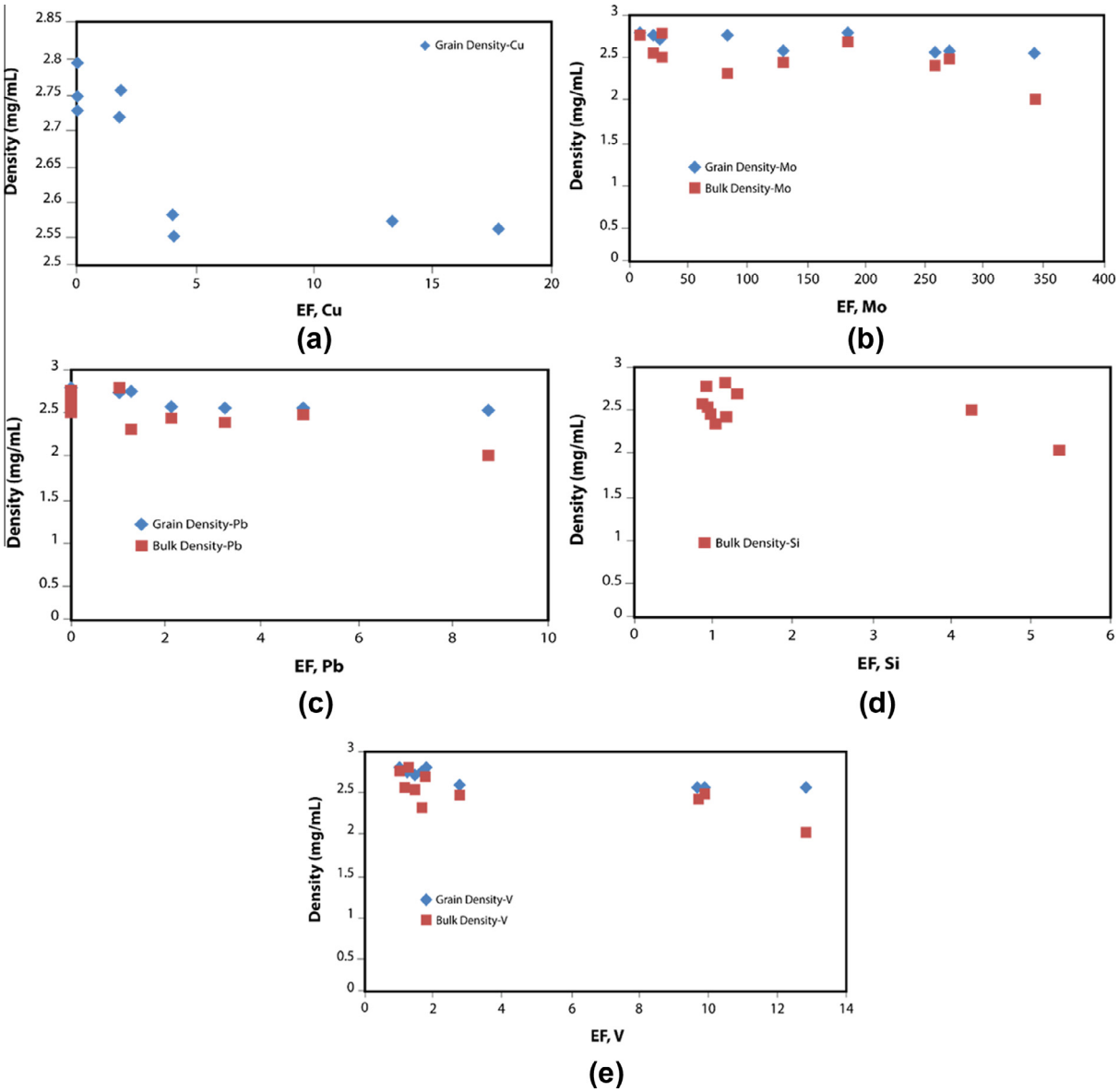

Fig. 6. Grain and bulk density vs the EFs of those correlated metals, (a) Cu; (b) Mo; (c) Pb; (d) Si; (e) V.

(Gasparik et al., 2014; Zhang et al., 2012). Gasparik et al. found that moisture has a significant negative impact on gas sorption capacity because of a competitive sorption between the gas and water molecules. In this study we did not dry the samples prior to tests and the samples may be equilibrated with moisture. Fig. 8 shows that the increase in CO_2 adsorption capacity parallels the absorption of CH_4. It suggests that during gas exposure process both CO_2 and CH_4 compete for same sorption sites on the shale samples. Since hydrophilic sites are occupied by water molecules it is most likely that both CO_2 and CH_4 approach the available hydrophobic and non-polar sites for adsorption.

At a given TOC concentration CO_2 has a higher adsorption capacity than CH_4 (Fig. 8). When extrapolating both CO_2 and CH_4 lines to TOC concentration of zero, the CO_2 shows a sorption of 0.088 mol/kg compared to 0.017 mol/kg for CH_4. This difference in adsorption in the absence of TOC suggests that in addition to organic adsorption sites, the CO_2 has other available adsorption sites possibly containing metal ions. It has been reported elsewhere that CO_2, as a Lewis Base, can form coordination species with metals (Llewellyn et al., 2008). In comparison, CH_4 is a completely non-polar molecule and favors solely Van der Waals association with the shale surfaces.

Fig. 9 shows that the maximum adsorption capacity of CO_2 is linearly proportional to that of CH_4 with a slope of 1. This result indicates that CO_2 and CH_4 share same adsorption sites on TOC. The difference in adsorption between CO_2 and CH_4 is mainly attributed to the excess adsorption of CO_2 on the non-TOC sites possibly metal ions.

Fig. 10 shows the ratio of adsorption capacity of CO_2 over CH_4 plotted against TOC. It is found that the ratios decrease with increased TOC content in general, which is consistent with the results reported in the literature (Sakurovs et al., 2012). Interestingly, two groups of adsorption capacity ratio of CO_2:CH_4 are identified depending on their corresponding TOC content. At low TOC (<2 wt%), the ratios are greater than 2 and has a linear positive relationship with TOC. When the TOC is higher than 2 wt%, the ratios do not show a linear trend with TOC, instead a scattering occurs around ratios 1.3–1.9. One hypothesis could be that at the lower TOC, CO_2 molecules form Lewis acid–base interactions with the organic-associated metals (i.e., Cu, Mo, Ni, Cr, V). The Lewis acid – base interactions specifically favor CO_2 adsorption over CH_4, leading to a high CO_2:CH_4 ratios in adsorption. With the increasing amount of TOC in shale, the Van der Waals force plays a major role in adsorption of both gases, which is indiscriminate to CO_2 and CH_4. Therefore, the CO_2:CH_4, ratios in adsorption remain insensitive to the TOC content. According to Sakurovs et al. (2012), this ratio is close to the ratio of the critical temperatures of both gases. The critical temperatures for CO_2 and CH_4 are 304.2 K and 190.5 K, respectively. The ratio of these critical temperatures 1.6 is located within the range of 1.3 to 1.9 as shown in Fig. 10.

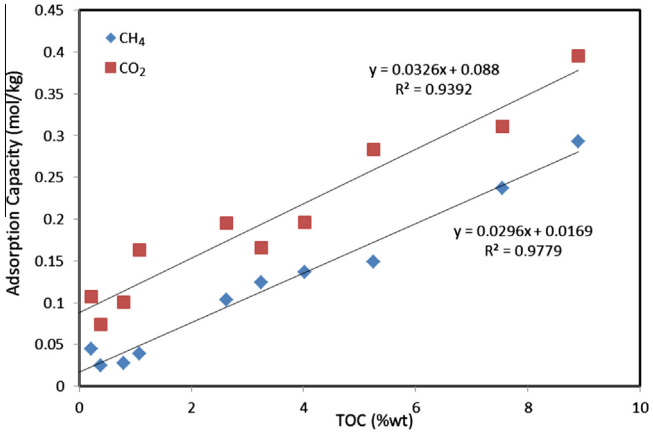

Fig. 8. CO_2 and CH_4 adsorption capacity as a function of TOC.

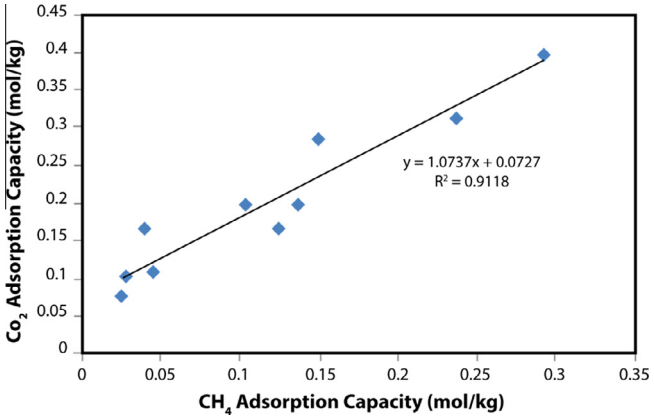

Fig. 9. CO_2 adsorption capacity versus CH_4 adsorption capacity.

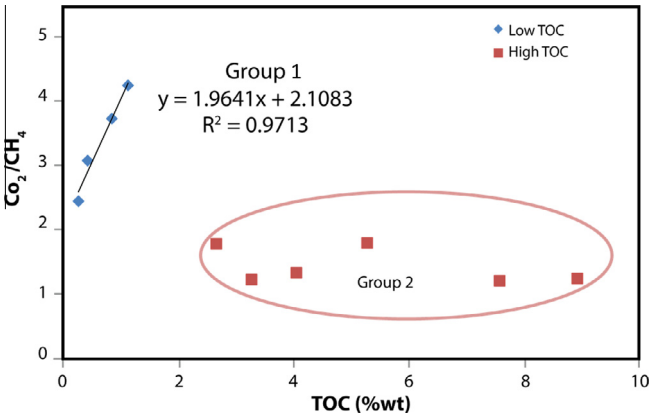

Fig. 10. The ratio of CO_2 over CH_4 as a function of TOC.

6. Summary

Ten outcrop shale samples were collected from seven locations in West Virginia, Virginia, Pennsylvania, and New York have been used in these studies. These samples were selected as proxies to improve understanding of shales from the producing natural gas reservoirs within the Appalachian Basin. XRD show the shale samples do not contain swelling clays in their composition. FTIR analyses indicate CO_2 has two distinct adsorption sites, inorganic and organic. Statistical analyses indicates that there is a strong correlation between the TOC and certain trace metals. TIC is statistically correlated with the carbonate metals, including As, Ba, Ca, Cd, Co, Cr, Fe, Mg, Mn, Na, Sr, and Ti, while TOC is correlated with Cu, K, and Ni. It is also observed that grain density increases as TOC decreases. Carbon dioxide and methane sorption isotherms on the shale samples were measured at 349 K (76 °C). The Langmuir equation provided a good fit for the maximum adsorption capacities for both CO_2 and CH_4. The adsorption capacities of both gases exhibit a linear relationship with TOC, which is consistent with the literature. However, CO_2 has a higher adsorption capacity than CH_4 and this increased adsorption of CO_2 appears to be due to contribution by non-TOC sites in the shale samples. This study brings insight in the interaction of CO_2 and CH_4 with shale and explores

the potential for long-term CO_2 storage in depleted natural gas reservoirs, while achieving enhanced gas recovery simultaneously.

Disclaimer

This technical effort was performed in support of the National Energy Technology Laboratory's ongoing research under the RES contract DE-FE0004000.

This project was funded by the Department of Energy, National Energy Technology Laboratory, an agency of the United States Government, through a support contract with URS Energy & Construction, Inc. Neither the United States Government nor any agency thereof, nor any of their employees, nor URS Energy & Construction, Inc., nor any of their employees, makes any warranty, expressed or implied, or assumes any legal liability or responsibility for the accuracy, completeness, or usefulness of any information, apparatus, product, or process disclosed, or represents that its use would not infringe privately owned rights. Reference herein to any specific commercial product, process, or service by trade name, trademark, manufacturer, or otherwise, does not necessarily constitute or imply its endorsement, recommendation, or favoring by the United States Government or any agency thereof. The views and opinions of authors expressed herein do not necessarily state or reflect those of the United States Government or any agency thereof.

Acknowledgments

This work was conducted by National Energy Technology Laboratory (NETL) research for the Department of Energy's Strategic Center for Coal and was funded by the Industrial Carbon Management Initiative (ICMI), an American Recovery and Re-Investment Act (ARRA)-funded project. Ms. Traci Rodosta (NETL Strategic Center for Coal, DOE Office of Fossil Energy) supported this project with her programmatic guidance and Dr. Ronald Breault coordinated federal research efforts on an ICMI task through the Carbon Capture Simulation and Storage Initiative project. Authors wish to acknowledge supports from Ms. Rodosta and Dr. Breault, as well acknowledge the technical input of Dr. George Guthrie, Dr. Tracy Bank, and ICMI Technical Director Dr. Geo Richards.

Appendix A. Supplementary data

Supplementary data associated with this article can be found, in the online version, at http://dx.doi.org/10.1016/j.juogr.2016.02.003.

References

Abrahim, G.M.S., Parker, R.J., 2008. Assessment of heavy metal enrichment factors and the degree of contamination in marine sediments from Tamaki Estuary, Auckland, New Zealand. Environ. Monit. Assess. 136, 227–238. http://dx.doi.org/10.1007/s10661-007-9678-2.

Aminian, K., Rodvelt, G., 2014. Evaluation of coalbed methane reservoirs. In: Thakur, P., Aminian, K., Schatzel, S. (Eds.), Coal Bed Methane: From Prospect to Pipeline. Elsevier, pp. 63–92.

Brumsack, H.J., 2006. The trace metal content of recent organic carbon-rich sediments: implications for Cretaceous black shale formation. Palaeogeogr. Palaeoclimatol. Palaeoecol. 232, 344–361. http://dx.doi.org/10.1016/j.palaeo.2005.05.011.

Busch, A., Alles, S., Gensterblum, Y., Prinz, D., Dewhurst, D.N., Raven, M.D., Stanjek, H., Krooss, B.M., 2008. Carbon dioxide storage potential of shales. Int. J. Greenhouse Gas Control 2, 297–308. http://dx.doi.org/10.1016/j.ijggc.2008.03.003.

Busch, A., Alles, S., Krooss, B.M., Stanjek, H., Dewhurst, D., 2009. Effects of physical sorption and chemical reactions of CO_2 in shaly caprocks. Energy Procedia 1, 3229–3235. http://dx.doi.org/10.1016/j.egypro.2009.02.107.

Cate, A.S., 1963. Lithostratigraphy of some Middle and Upper Devonian rocks in the subsurface of southwestern Pennsylvania. In: Shepps, V.C. (Ed.), Symposium on Middle and Upper Devonian Stratigraphy of Pennsylvania and Adjacent States: Pennsylvania Geological Survey General Geology Report, 4th Series, pp. 229–240.

Chen, S., Zhu, Y., Qin, Y., Wang, H., Liu, H., 2014. Reservoir evaluation of the Lower Silurian Longmaxi Formation shale gas in the southern Sichuan Basin of China. Mar. Pet. Geol. 57, 619–630. http://dx.doi.org/10.1016/j.marpetgeo.2014.07.008.

de Witt, W.J., Roen, J.B., Wallace, L.G., 1993. Stratigraphy of Devonian black shales and associated rocks in the Appalachian basin. In: Roen, J.B., Kepferle, R.C. (Eds.), Petroleum Geology of the Devonian and Mississippian Black Shale of Eastern North America. Geological Survey Bulletin, Washington, U.S, pp. B1–B57.

Gasparik, M., Bertier, P., Gensterblum, Y., Ghanizadeh, A., Krooss, B.M., Littke, R., 2014. Geological controls on the methane storage capacity in organic-rich shales. Int. J. Coal Geol. 123, 34–51. http://dx.doi.org/10.1016/j.coal.2013.06.010.

Godec, M., Koperna, G., Petrusak, R., Oudinot, A., 2014. Enhanced gas recovery and CO_2 storage in gas shales: a summary review of its status and potential. Energy Procedia 63, 5849–5857. http://dx.doi.org/10.1016/j.egypro.2014.11.618.

Godec, M., Koperna, G., Petrusak, R., Oudinot, A., 2013. Potential for enhanced gas recovery and CO_2 storage in the Marcellus Shale in the Eastern United States. Int. J. Coal Geol. 118, 95–104. http://dx.doi.org/10.1016/j.coal.2013.05.007.

Goodman, A.L., 2009. A comparison study of carbon dioxide adsorption on polydimethylsiloxane, silica gel, and illinois no. 6 coal using in situ infrared spectroscopy. Energy & Fuels 23, 1101–1106. http://dx.doi.org/10.1021/ef8008025.

Hosterman, J.W., Whitlow, S.I., 1981. Munsell color value as related to organic carbon in Devonian shale of Appalachian basin. Am. Assoc. Pet. Geol. Bull. 65, 333–335. http://dx.doi.org/10.1306/2F9197CE-16CE-11D7-8645000102C1865D.

Hur, T.-B., Baltrus, J.P., Howard, B.H., Harbert, W.P., Romanov, V.N., 2013. Carbonate formation in Wyoming montmorillonite under high pressure carbon dioxide. Int. J. Greenhouse Gas Control 13, 149–155. http://dx.doi.org/10.1016/j.ijggc.2012.12.001.

Kang, S.M., Fathi, E., Ambrose, R.J., Akkutlu, I.Y., Sigal, R.F., 2011. Carbon Dioxide Storage Capacity of Organic-Rich Shales, 1–14.

Klinkenberg, L.J., 1941. The permeability of porous media to liquids and gases. API Drill. Prod. Pract., 200–2013

Krukowski, E.G., Goodman, A., Rother, G., Ilton, E.S., Guthrie, G., Bodnar, R.J., 2015. FT-IR study of CO_2 interaction with Na+ exchanged montmorillonite. Appl. Clay Sci. 114, 61–68. http://dx.doi.org/10.1016/j.clay.2015.05.005.

Li, C., Li, G.Q., Xin, Q., 1994. FT-IR spectroscopic studies of methane adsorption on magnesium oxide. J. Phys. Chem. A 98, 1933–1938. http://dx.doi.org/10.1021/j100058a036.

Llewellyn, P.L., Bourrelly, S., Serre, C., Vimont, A., Daturi, M., Hamon, L., Weireld, G. De, Chang, J., Hong, D., Hwang, Y.K., Jhung, S.H., 2008. High uptakes of CO_2 and CH_4 in mesoporous metals organic frameworks MIL-100 and MIL-101. Adsorpt. J. Int. Adsorpt. Soc., 7245–7250

Loring, J.S., Ilton, E.S., Thompson, C.J., Martin, P.F., Rosso, K.M., Felmy, A.R., Schaef, H. T., 2014. In situ study of CO_2 and H_2O partitioning between Na – montmorillonite and variably wet supercritical carbon dioxide. Langmuir 30, 6120–6128.

Loucks, R.G., Ruppel, S., Reed, R.M., Hammes, U., 2011. Origin and classification of pores in mudstones from shale-gas systems. In: AAPG International Conference and Exhibition. Milan, Italy.

Martin, P.E., Barker, E.F., 1932. The infrared absorption spectrum of carbon dioxide. Phys. Rev. 1150, 291–303.

McGinnis, C.E., Jain, J.C., Neal, C.R., 1997. Characterisation of memory effects and development of an effective wash protocol for the measurement of petrogenetically critical trace elements in geological samples by ICP-MS. Geostand. Newsl. 21, 289–305. http://dx.doi.org/10.1111/j.1751-908X.1997.tb00677.x.

Molecular Database, The Virtual Planetary Laboratory [WWW Document], 2015. Virtual Planet. Lab. NASA Astrobiol. Inst. URL http://vpl.astro.washington.edu/spectra/allmoleculeslist.htm.

Narinesingh, J., Alexander, D., 2014. CO_2 enhanced gas recovery and geologic sequestration in condensate reservoir: a simulation study of the effects of injection pressure on condensate recovery from reservoir and CO_2 storage efficiency. Energy Procedia 63, 3107–3115. http://dx.doi.org/10.1016/j.egypro.2014.11.334.

Neff, J.M., McKelvie, S., Ayers, R.C.J., 2000. Environmental Impacts of Synthetic Based Drilling Fluids. OCS Study MMS 2000-64. U.S. Dept. of the Interior, Minerals Management Service, Gulf of Mexico OCS Program, New Orleans, LA.

Nuttal, B.C., Eble, C.F., Bustin, R.M., Drahovzal, J.A., 2005. Analysis of Devonian Black Shales in Kentucky for Potential Carbon Dioxide Sequestration and Enhanced Natural Gas Production. DE-FC26-02NT41442, Kentucky Geological Survey 228 Mining and Mineral Resources Building University of Kentucky Lexington, Kentucky 40506-0107. doi: 10.1016/B978-008044704-9/50306-2.

Orr, F.M., 2009. Onshore geologic storage of CO_2. Science 325, 1656–1658. http://dx.doi.org/10.1126/science.1175677.

Pi, D.H., Liu, C.Q., Shields-Zhou, G.A., Jiang, S.Y., 2013. Trace and rare earth element geochemistry of black shale and kerogen in the early Cambrian Niutitang Formation in Guizhou province, South China: constraints for redox environments and origin of metal enrichments. Precambrian Res. 225, 218–229. http://dx.doi.org/10.1016/j.precamres.2011.07.004.

Poppe, L.J., Paskevich, V.F., Hathaway, J.C., Blackwood, D.S., 2001. A laboratory manual for X-ray powder diffraction. U. S. Geol. Surv. Open-File Rep. 01–041, 88.

Repetski, J.E., Over, D.J., Rotter, D.L., 2012. Conodonts from the Marcellus Shale interval in the Central Appalachians. In: Geological Society of America Abstracts with Programs. Colorado, p. 2.

Roen, J.B., Hosterman, J.W., 1982. Misuse of the term "bentonite" for ash beds of Devonian age in the Appalachian basin. Bull. Geol. Soc. Am. 93, 921–925, doi: 10.1130/0016-7606(1982)93<921:MOTTBF>2.0.CO;2.

Romanov, V.N., 2013. Evidence of irreversible CO_2 intercalation in montmorillonite. Int. J. Greenhouse Gas Control 14, 220–226. http://dx.doi.org/10.1016/j.ijggc.2013.01.022.

Sakurovs, R., Day, S., Weir, S., 2012. Relationships between the sorption behaviour of methane, carbon dioxide, nitrogen and ethane on coals. Fuel 97, 725–729. http://dx.doi.org/10.1016/j.fuel.2012.03.014.

Sakurovs, R., Day, S., Weir, S., Duffy, G., 2008. Temperature dependence of sorption of gases by coals and charcoals. Int. J. Coal Geol. 73, 250–258. http://dx.doi.org/10.1016/j.coal.2007.05.001.

Sakurovs, R., Day, S., Weir, S., Duffy, G., 2007. Application of a modified Dubinin–Radushkevich equation to adsorption of gases by coals under supercritical conditions. Energy Fuels 21, 992–997. http://dx.doi.org/10.1021/ef0600614.

Schaef, H.T., Davidson, C.L., Owen, A.T., Miller, Q.R.S., Loring, J.S., Thompson, C.J., Bacon, D.H., Glezakou, V.A., McGrail, B.P., 2014. CO_2 utilization and storage in shale gas reservoirs: experimental results and economic impacts. Energy Procedia 63, 7844–7851. http://dx.doi.org/10.1016/j.egypro.2014.11.819.

Schepers, K., Nuttall, B., Oudinot, A., Gonzalez, R., 2009. Reservoir modeling and simulation of the Devonian gas shale of Eastern Kentucky for enhanced gas recovery and CO_2 storage. In: Proc. SPE Int. Conf. CO_2 Capture, Storage, Util. doi: 10.2118/126620-MS.

Soeder, D.J., 2012. Shale gas development in the United States. In: Al-Megren, H.A. (Ed.), Advances in Natural Gas Technology. Intechopen, pp. 3–28. doi: 10.5772/2324.

Soeder, D.J., 1988. Porosity and permeability of eastern Devonian gas shale. SPE Form. Eval. 3, 116–124. http://dx.doi.org/10.2118/15213-PA.

Taylor, R., 1990. Interpretation of the correlation coefficient: a basic review. J. Diagn. Med. Sonogr. 6, 35–39. http://dx.doi.org/10.1177/875647939000600106.

Vine, J.D., Tourtel, E.B., 1970. Geochemistry of black shale deposits – a summary report. Econ. Geol. 65, 253–272. http://dx.doi.org/10.2113/gsecongeo.65.3.253.

Walker-Milani, M.E., 2011. Outcrop Lithostratigraphy and Petrophysics of the Middle Devonian Marcellus Shale in West Virginia and Adjacent States. West Virginia University.

Wilde, P., Lyons, T.W., Quinby-Hunt, M.S., 2004. Organic carbon proxies in black shales: molybdenum. Chem. Geol. 206, 167–176. http://dx.doi.org/10.1016/j.chemgeo.2003.12.005.

Yang, Y., Liang, C., Zhang, J., Jiang, Z., Tang, X., 2015. A developmental model of lacustrine shale gas genesis: a case from T3y7 shale in the Ordos Basin, China. J. Nat. Gas Sci. Eng. 22, 395–405. http://dx.doi.org/10.1016/j.jngse.2014.12.014.

Zhang, D.F., Cui, Y.J., Liu, B., Li, S.G., Song, W.L., Lin, W.G., 2011. Supercritical pure methane and CO_2 adsorption on various rank coals of China: experiments and modeling. Energy Fuels 25, 1891–1899. http://dx.doi.org/10.1021/ef101149d.

Zhang, T., Ellis, G.S., Ruppel, S.C., Milliken, K., Yang, R., 2012. Effect of organic-matter type and thermal maturity on methane adsorption in shale-gas systems. Org. Geochem. 47, 120–131. http://dx.doi.org/10.1016/j.orggeochem.2012.03.012.

Zhang, Y., Liu, S., Song, Y., Zhao, J., Tang, L., Xing, W., Jian, W., Liu, Z., Zhan, Y., 2014. Experimental investigation of CO_2-CH_4 displacement and dispersion in sand pack for enhanced gas recovery. Energy Procedia 61, 393–397. http://dx.doi.org/10.1016/j.egypro.2014.11.1133.